

Reaction Mechanism of Ru(II) Piano-Stool Complexes: Umbrella Sampling QM/MM MD Study

Zdeněk Futera^[a] and Jaroslav V. Burda^{*[b]}

Biologically relevant interactions of piano-stool ruthenium(II) complexes with ds-DNA are studied in this article by hybrid quantum mechanics—molecular mechanics (QM/MM) computational technique. The whole reaction mechanism is divided into three phases: (i) hydration of the $[\text{Ru}^{\text{II}}(\eta^6\text{-benzene})(\text{en})\text{Cl}]^+$ complex, (ii) monoadduct formation between the resulting aqua-Ru(II) complex and N7 position of one of the guanines in the ds-DNA oligomer, and (iii) formation of the intrastrand Ru(II) bridge (cross-link) between two adjacent guanines. Free energy profiles of all the reactions are explored by QM/MM MD umbrella sampling approach where the Ru(II) complex and two guanines represent a quantum core, which is described by density functional theory methods. The combined QM/MM scheme is realized by our own software, which was developed

to couple several quantum chemical programs (in this study Gaussian 09) and Amber 11 package. Calculated free energy barriers of the both ruthenium hydration and Ru(II)-N7(G) DNA binding process are in good agreement with experimentally measured rate constants. Then, this method was used to study the possibility of cross-link formation. One feasible pathway leading to Ru(II) guanine-guanine cross-link with synchronous releasing of the benzene ligand is predicted. The cross-linking is an exergonic process with the energy barrier lower than for the monoadduct reaction of Ru(II) complex with ds-DNA. © 2014 Wiley Periodicals, Inc.

DOI: 10.1002/jcc.23639

Introduction

The interactions of transition metals with (bio)organic molecules are well-known and abundantly exploited in many branches of chemistry and related fields. Since a lot of various metals are naturally present in living organisms, it is not surprising that these compounds are often used in pharmacology and medicine.^[1–4] Probably, the best known and rapidly developing area is a utilization of heavy metal compounds in oncology. Diamminedichloroplatinum(II) complex, known as cisplatin (Fig. 1a), was the first transition metal complex approved for anticancer treatment and up to present date is applied in 70% of chemotherapeutically treated patients.^[5,6]

Mechanism of cisplatin activity was intensively studied experimentally^[7–10] as well as theoretically^[11–22] using computer simulations and it is believed to be sufficiently known nowadays. Cisplatin is administered intravenously and then it passes cellular membrane and enters the cancer cell from bloodstream. First process after entering the cell is a replacement of one or both chloride ligands by water molecules. The hydration reaction is driven by a substantially reduced concentration of chloride anions inside the cell in comparison to intercellular environment. Resulting Pt(II) aqua complex is much more reactive than cisplatin itself and can interact with various nucleophilic sites found on peptides or nucleotides. The most important step for the anticancer activity is the interaction with DNA in the cell nucleus. Cisplatin preferably binds to N7 nitrogen of guanosine that is well accessible from the major groove of the DNA double helix. If there are some adjacent guanines in the DNA sequence, cisplatin can create the so-called cross-linked structure, that is Pt-bridge between two N7 nitrogens of guanines.^[23,24] In this case, both intra-

strand or interstrand cross-links are possible; however, the former ones are highly preferred. The cross-linked structure is very stable and leads to local DNA deformation connected with unwinding and bending of the helix structure. Such structural changes are recognized by high-mobility-group proteins and finally can lead to apoptosis, controlled cell death.^[25]

Successful application of cisplatin in the antitumor therapy led to intensive investigation in organometallic research looking for compounds, which would have better activity and less toxic side effects.^[26,27] Several such complexes were found and approved for the medical practice. Recently, promising group of ruthenium(II) compounds, the so-called “piano-stool” complexes, were examined in several laboratories.^[28,29] In this study, we explore reactivity of the $[\text{Ru}^{\text{II}}(\eta^6\text{-benzene})(\text{en})\text{Cl}]^+$ complex (Fig. 1b) as a representative of this group. It was experimentally observed that the Ru(II) complex undergoes hydration reaction, in analogy to cisplatin, and subsequently it interacts with DNA. Preference for N7 binding position of guanine was proven too.^[30–35] However, full mechanism of activity remains still unknown.

In this computational study, we employ a hybrid quantum mechanics—molecular mechanics approach (QM/MM) to investigate processes of the $[\text{Ru}^{\text{II}}(\eta^6\text{-benzene})(\text{en})\text{Cl}]^+$ complex in

[a] Z. Futera

Department of Chemistry, Faculty of Science and Technology, Keio University, 3-14-1 Hiyoshi, Kohoku-ku, Yokohama 223-8522, Japan

[b] J. V. Burda

Faculty of Mathematics and Physics, Charles University in Prague, Ke Karlovu 3, 121 16 Prague 2, Czech Republic
E-mail: burda@karlov.mff.cuni.cz

Contract grant sponsor: Czech Republic (project No P208/12/0622)

© 2014 Wiley Periodicals, Inc.

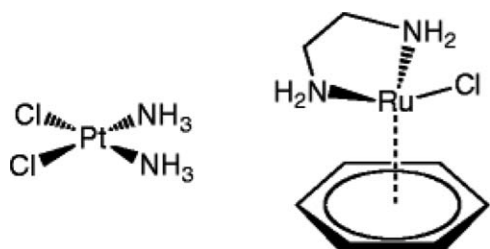


Figure 1. Structural formula of (a) cisplatin and (b) $[\text{Ru}^{\text{II}}(\eta^6\text{-benzene})(\text{en})\text{Cl}]^+$ complex.

relation to cellular environment. These reactions can be divided into three phases: (i) hydration reaction (**R0**), (ii) binding to DNA in N7 guanine position—monoadduct formation (**R1**), and finally (iii) intrastrand cross-linking between two adjacent guanines (**R2**). For the hydration reaction (replacement of the chloride ligand by a water molecule), there is reliable experimental support, which allow us to verify accuracy of our computational models. Subsequent binding to N7 guanine in DNA can proceed by two different reaction pathways as it was already shown in Refs. [36,37]. Possibility of the both pathways is reinvestigated also in this study using QM/MM approach. The cross-link formation, although not observed experimentally yet, was already suggested in our previous work^[38]. The free energy profiles of all the reactions are constructed by both umbrella integration (UI) and weighted histogram analysis method (WHAM) from the QM/MM MD umbrella sampling trajectories.

The article is organized as follows: QM/MM computational model is briefly described in Computational Methods section together with umbrella sampling technique used for the free energy determination. Also, the two methods, UI and WHAM used for constructing the free energy profile from biased MD trajectories are described here. The detailed description is connected with the fact that all the QM/MM interface together with consequent analyses were coded into new program QMS by one of the authors (Z.F.). The main part of the article deals with presentation of obtained results for the above mentioned reactions **R0**, **R1**, and **R2** of the ruthenium(II) complex.

Computational Methods

The hybrid QM/MM computational technique is used in this work to optimize the computational model and perform Born–Oppenheimer molecular dynamics. QM/MM is implemented in a new program interface called QMS, which can couple several existing quantum mechanical (QM) programs and molecular mechanical (MM) software (Gaussian 09^[39] and Amber 8^[40] in this study). The QMS code can also employ GAMESS,^[41] Turbomole,^[42] and Molpro^[43] packages.

QM/MM technique

The hybrid QM/MM method is popular approach for treating large computational models where chemical changes occur only in a relatively small region. This area can be evaluated by an accurate but computational demanding QM method while

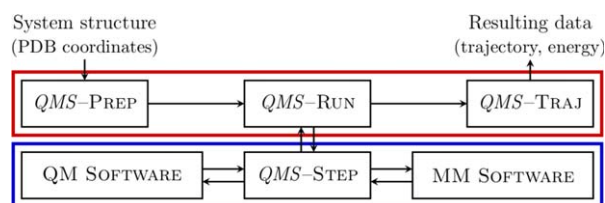


Figure 2. Data flow diagram and modular structure of QMS program layer. [Color figure can be viewed in the online issue, which is available at wileyonlinelibrary.com.]

the remaining part of the system is described by MM. This is typical QM/MM partitioning of the studied system S into inner part I surrounded by outer part O . The boundary between I and O involving possible link atoms is further marked as L .

However, there are two commonly used approaches to evaluate total QM/MM energy of the studied system. First, the so-called additive scheme is a straightforward summation of energy contributions of the inner and outer parts and their mutual interaction:

$$E_{\text{QMMM}}(S) = E_{\text{MM}}(O) + E_{\text{QM}}(I+L) + E_{\text{QM-MM}}(S). \quad (1)$$

The additive scheme can be applied in program codes that have direct access to all MM and QM data and thus it can evaluate the last term in eq. (1) effectively. However, for software interfaces dealing with standalone QM and MM programs, a subtractive scheme proposed by Morokuma and coworkers^[44] is more feasible to use.

$$E_{\text{QMMM}}(S) = E_{\text{MM}}(S) + E_{\text{QM}}(I+L) - E_{\text{MM}}(I+L). \quad (2)$$

In this case, the mutual interaction of the inner and outer part is obtained implicitly by replacing the MM energy contribution of the inner part by its QM energy.

Implementation

We implemented the subtracted energy scheme of the QM/MM method as described above into a new software called QMS. This QMS program package is designed as an interface that is able to couple MM techniques included in Amber^[40] with QM tools for obtaining electronic structure—Gaussian,^[39] GAMESS,^[41] Molpro,^[43] or Turbomole.^[42] The program is designed as a set of cooperating modules as it is illustrated in data flow chart in Figure 2. The main module QMS-step is parallelized for efficient employment of computational recourses. In this way, QMS can work in two different modes and perform QM/MM energy optimization or MD simulation.

In the geometry optimization mode, three popular methods are coded: steepest descents, conjugate gradient, and limited-memory BFGS algorithm.^[45] For Born–Openheimer MD, the velocity Verlet algorithm^[46,47] is used together with Andersen^[48] or Berendsen thermostat^[49] to run dynamics in NVT ensemble. This is supplemented by automatic sampling techniques and because the restraining of internal and/or Cartesian coordinates is also available, the QMS code can be used for

Table 1. Activation barriers and reaction energies (kcal/mol) for the **R1** process.

Reaction/Methods	QM(C-PCM)		ONIOM		QM/MM _{MD}		QM/MM _{corr}	
	ΔG_a	ΔG_r	ΔG_a	ΔG_r	ΔG_a	ΔG_r	ΔG_a	ΔG_r
R _{R1} → P _{R1}	29.1	−1.3	26.5	−12.2	15.3	−1.8	22.5	−4.5
R _{R1} → I _{R1}	28.5	1.4	27.8	−1.1	15.7	9.2	21.1	7.8
I _{R1} → P _{R1}	34.7	−2.7	29.3	−11.1	4.8	−11.3	10.8	−11.2

QM/MM_{MD} stands for umbrella sampling result at the B97D/LANL2DZ level and QM/MM_{corr} are the values corrected by FEP at the B3LYP/6-31++G(d,p) level. For a comparison, ONIOM values from Ref. [38] are shown as well.

the Umbrella Sampling free energy calculations as discussed below.

Free energy determination

The free energy profile of chemical reaction is very important characteristics; the difference of reaction minima decides about its spontaneity while the height of energy barrier correlates directly with the reaction kinetics. However, from computational point of view, the free energy calculation is a difficult task as it contains entropy contributions and thus a configurational space has to be properly sampled. Direct approach is very demanding and, practically, it cannot be used with QM/MM MD. Therefore, several sophisticated methods with enhanced sampling were developed.^[50] In this work, we use the so-called umbrella sampling technique.

In the umbrella sampling,^[51–53] a reaction coordinate ξ is divided into N_w windows, which are then sampled individually. To ensure efficient sampling, a bias potential w_i is applied in each window to restrain the reaction coordinate, typically in a harmonic form, $w_i(\xi) = 1/2 K_i (\xi - \xi_i)^2$. Biased distribution in each window, P_i^b , is obtained from the MD simulation as a histogram of the reaction coordinate, which is connected with the searched free energy.

$$A_i(\xi) = -\frac{1}{\beta} \ln P_i^b(\xi) - w_i(\xi) + F_i. \quad (3)$$

Term $F_i = -\frac{1}{\beta} \ln \langle \exp[-\beta w_i] \rangle$, where sharp brackets represent statistical averaging, is a free energy shift in i -th window caused by bias potential w_i .

In this work, we use WHAM^[54,55] to calculate the free energy shifts from overlaps of P_i^b distributions. Total unbiased distribution, which is directly connected with free energy, can be constructed as a weighted average of the biased distributions emerging from MD simulations.

$$P^u(\xi) = \sum_{i=1}^{N_w} P_i(\xi) P_i^b(\xi), \quad (4)$$

with the weights p_i chosen to minimize statistical error of $P^u(\xi)$. This gives the set of nonlinear equations that are coupled by free energy shifts F_i and thus they have to be solved iteratively. Accuracy of this method is strongly dependent on P_i^b overlaps; nevertheless, the method can be in principle used for analysis of Umbrella Sampling simulations with any type of bias potential.

UI^[56,57] is an analytic alternative to the WHAM method, which is applicable if the harmonic bias potentials were used for restraining umbrella sampling simulations and the resulting P_i^b distributions can be approximated by Gaussian functions $G(\xi_i^b, \sigma_i^b)$. In such case, the mean force can be directly constructed.

$$\frac{\partial A}{\partial \xi} = \sum_{i=1}^{N_w} \frac{N_i P_i^b(\xi)}{\sum_{i=1}^{N_w} N_i P_i^b(\xi)} \left[\frac{\xi - \xi_i^b}{\beta (\sigma_i^b)^2} - K_i (\xi - \xi_i^b) \right]. \quad (5)$$

Comparing to WHAM, UI technique does not require overlapping distributions although they are desirable for higher accuracy. As a result of approximating P_i^b by Gaussian normal distributions, the final potential of mean force is always represented by a smooth curve.

Computational Models

QM/MM model for the hydration reaction

The replacement of the chloro ligand of the studied Ru(II) complex by water occurs in aqueous environment of a cell. No other molecules like nucleic acids or proteins were considered at this step. Therefore, the QM/MM model of the $[\text{Ru}^{\text{II}}(\eta^6\text{-benzene})(\text{en})\text{Cl}]^+$ complex solvated by explicit water molecules was built by LEaP program.^[58] The complex together with one water molecule participating in the **R0** reaction was defined as the QM part of the system. Structure of the complex was parameterized by General Amber Force Field (GAFF)^[59] with Restrained Electrostatic Potential (RESP) charges^[60–63] fitted from HF/6-31G(d) electron density calculated by Gaussian 09.^[39] Rectangular box ($a = 33.633 \text{ \AA}$, $b = 31.547 \text{ \AA}$, $c = 30.918 \text{ \AA}$) filled with 1111 TIP3P^[64] water molecules and one Cl^- counterion was used as a simulation cell in program Amber 8.^[40] The box parameters were obtained by NPT ($p = 1 \text{ atm}$) MD density equilibration preceded by smooth NVT ($T = 298.15 \text{ K}$) annealing. Finally, production QM/MM MD umbrella sampling simulations were performed by the QMS program at room temperature controlled by Berendsen thermostat.^[49] The reaction coordinate for this calculation was defined as $\xi = \Delta R_{\text{Cl}} / (\Delta R_{\text{Aq}} + \Delta R_{\text{Cl}})$ where $\Delta R_x = R_x - R_x^{\text{ref}}$ are displacements of Ru(II)–X distance (R_x) from its reference value R_x^{ref} . The lengths of Ru(II)–Cl and Ru(II)–Aq bonds were chosen from optimized QM/MM model were chosen as references (see Supporting Information, Table S1 for numerical values) to scale ξ conveniently into $[0,1]$ interval.

This interval was divided equidistantly into 17 windows and individual umbrella sampling MD simulations were performed for 5 ps. The preset Ru(II)—Cl and Ru(II)—Aq bond lengths were restrained by harmonic potentials with force constant 50 kcal/mol/Å² in each window. Convergence of the biased distributions P_i^b and the resulting free energy profile $A(\xi)$ was carefully checked, and the simulation time was increased if necessary.

The QM part of the model was described by density functional theory (DFT) with hybrid B3LYP functional. This setting is based on our previous work where accuracy of several different methods were checked with respect to experimental data (see Ref. [36] for more details). We use 6-31G(d) basis set for geometry optimization resp. MD and larger 6-31++G(2df,2pd) for molecular analysis. Stuttgart–Dresden pseudopotential (SDD)^[65–67] are used for 10 electrons on Cl and 28 core electrons on Ru. Original set of pseudoorbitals is augmented by polarization functions with exponents $\alpha_r(\text{Ru}) = 1.29$ and $\alpha_d(\text{Cl}) = 0.618$ for optimization. In single-point calculations (SP), diffuse functions are added to the (2fg,2df) basis set: $\alpha_s(\text{Ru}) = 0.008$, $\alpha_p(\text{Ru}) = 0.011$, $\alpha_d(\text{Ru}) = 0.025$, $\alpha_f(\text{Ru}) = 2.233$, $\alpha_h(\text{Ru}) = 0.6503$, $\alpha_g(\text{Ru}) = 1.4222$, $\alpha_s(\text{Cl}) = 0.09$, $\alpha_p(\text{Cl}) = 0.0075$, $\alpha_d(\text{Cl}) = 1.1898$, $\alpha_f(\text{Cl}) = 0.3681$, and $\alpha_h(\text{Cl}) = 0.7062$. In order to be consistent with larger QM parts in subsequent reactions (**R1**, and **R2**), lower level calculations (B97D/LANL2DZ) were performed as well. Electrostatic QM/MM embedding was applied for all calculations in this work.

QM/MM model of Ru(II) interacting with ds-DNA

In contrast to the hydration reaction, ruthenium binding to DNA and subsequent cross-link formation requires more complex computational model, which includes also oligonucleotide of DNA. Based on our previous ONIOM study,^[38] the QM/MM model with B-DNA oligonucleotide in explicit water box was prepared. The decamer of the ds-DNA structure with a sequence 5'-AATGG*G*ACCT-3' was built using the NucGen utility of AmberTools 8 package and parameterized by FF03^[68] force field from Amber 11.^[69] 18 Na⁺ counterions were used for sugar-phosphate backbone charge neutralization, explicit TIP3P water molecules were added and this "DNA solution" was relaxed by 100 ps MD run. After that, the DNA structure was extracted, and the hydrated Ru(II)²⁺ complex obtained as product of the previous reaction step was docked to the central guanine pair (signed by stars in the above mentioned sequence). Additional 16 Na⁺ cations were added together with 4000 TIP3P water molecules, and the whole box was equilibrated to the room temperature in NVT canonical ensemble followed by compression to pressure 1 atm in NPT ensemble. Final rectangular box (a = 45.641 Å, b = 59.046 Å, c = 47.345 Å) was kept fixed in all subsequent calculations. Link-atom approach was used to treat N9(G)-C1'(S) glycosidic bond between guanine (G) and deoxyribose (S) at the QM-MM boundary. The N9(G) nitrogen was cupped by hydrogen using scaling factor $\alpha_L = 1.464$. In the QM/MM partitioning, the Ru(II) complex and the two starred guanines were included in the QM part while all the rest of the model was treated by

empirical force field in MM calculations as it is shown in Figure 3.

B97D functional with dispersion correction was used to describe stacking interaction between two guanines in the QM part (at least qualitatively) correctly. On the other hand, smaller basis set had to be chosen (LANL2DZ pseudopotentials^[70–72] + D95V on first row atoms^[73] for all atoms in the QM part instead of the more demanding SDD/6-31G(d) description used in the preceding model. However, this level of theory was used for the geometry optimization of the full QM/MM model to discuss equilibrium structure parameters. The same optimization procedure as in Ref. [38] was applied here. Partial charges, QTAIM analysis,^[74–76] and binding energy (BE) decompositions were performed for the quantum cores using the B3LYP/SDD/6-31++G(d,p) model.

The umbrella sampling calculations were performed with the reaction coordinate defined analogically to **R0** reaction and analyzed by WHAM as well as UI. To increase accuracy of free energy differences, QM/MM energy of the model was reevaluated at B3LYP/SDD/6-31++G(d,p) level during the MD sampling to correct the $A(\xi)$ by free-energy perturbation (FEP)^[50] approach

$$\Delta G_{\text{LAN}}^{\text{SDD}} = G_{\text{SDD}} - G_{\text{LAN}} = k_B T \ln \left\langle \exp \left[-\frac{E_{\text{SDD}} - E_{\text{LAN}}}{k_B T} \right] \right\rangle_{\text{LAN}} \quad (6)$$

Results

Hydration reaction

The [Ru^{II}(η⁶-benzene)(en)Cl]⁺ complex in supermolecule with remote water represents reactant (**R_{RO}**, Fig. 4a) in hydration that proceeds when the complex passes cellular membrane and enters the cell. From UV-vis spectrometry measurements, it is known that the Ru(II) hydration is endothermic reaction, which occurs with the rate constant $k = (1.98 \pm 0.02) 10^{-3} \text{ s}^{-1}$.^[77] This value corresponds, supposing validity of Eyring's transition state theory (TST), to the activation barrier of 21.1 kcal/mol and thus it can be used for accuracy calibration of our calculations.

The reaction **R0** proceeds through the stationary points shown in Figure 4 where definition of key atoms can be noticed. The hydration is single barrier process during which the chloro ligand is released from the **R_{RO}** complex and substituted by the water molecule via associative mechanism. That means, the Cl[−] ligand is released simultaneously with strengthening of the aqua ligand binding to Ru(II). Regardless the fact that both ligands are very weakly bonded in TS structure, the corresponding imaginary frequency has the character of antisymmetric stretching vibrational mode of Cl—Ru—O well-known, for example from vibrational spectrum of water molecule. The **R0** process was investigated by static QM calculations both in gas phase and in implicit solvent model in [36] and these data are consistent with QM/MM results obtained in this study (see Supporting Information, Tables S1–S3 for details). The most strongly coordinated to the Ru cation is the ethylenediamine ligand (en) with binding energy (BE) between

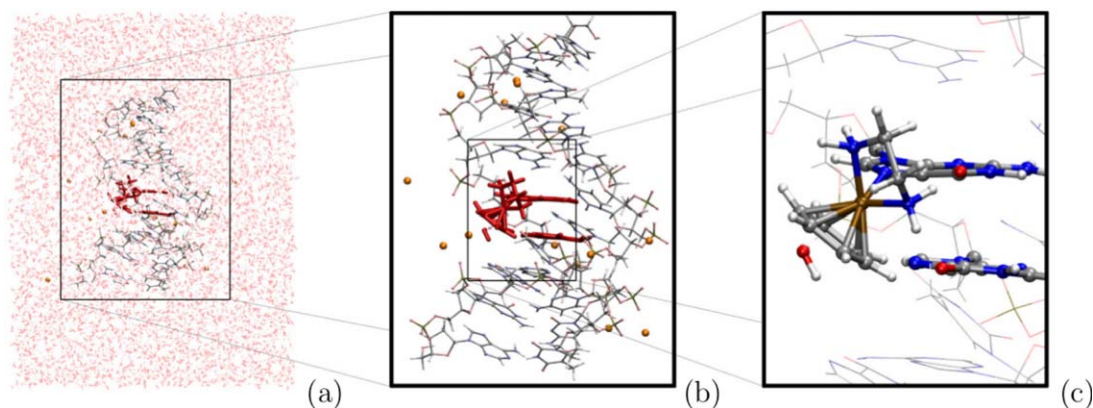


Figure 3. QM/MM computational model with periodic TIP3P water box (a), extracted DNA structure with coordinated Ru(II) complex and Na⁺ cations (b), and detailed insight into the QM part of the system (c).

100 and 110 kcal/mol. On the other hand, the η^6 -coordinated benzene ligand interacts with central Ru(II) relatively weakly, with BE varying between 73 and 88 kcal/mol.

As for the interaction of chloro and aqua ligand, there is the same trend along the reaction coordinate; the electron density

donated to Ru(II) by Cl⁻ is higher than the density donated by oxygen of the aqua ligand.

Since the present work concentrates on the interaction of Ru(II) complexes with DNA, the QM/MM technique with explicit water box represents a much more realistic model.

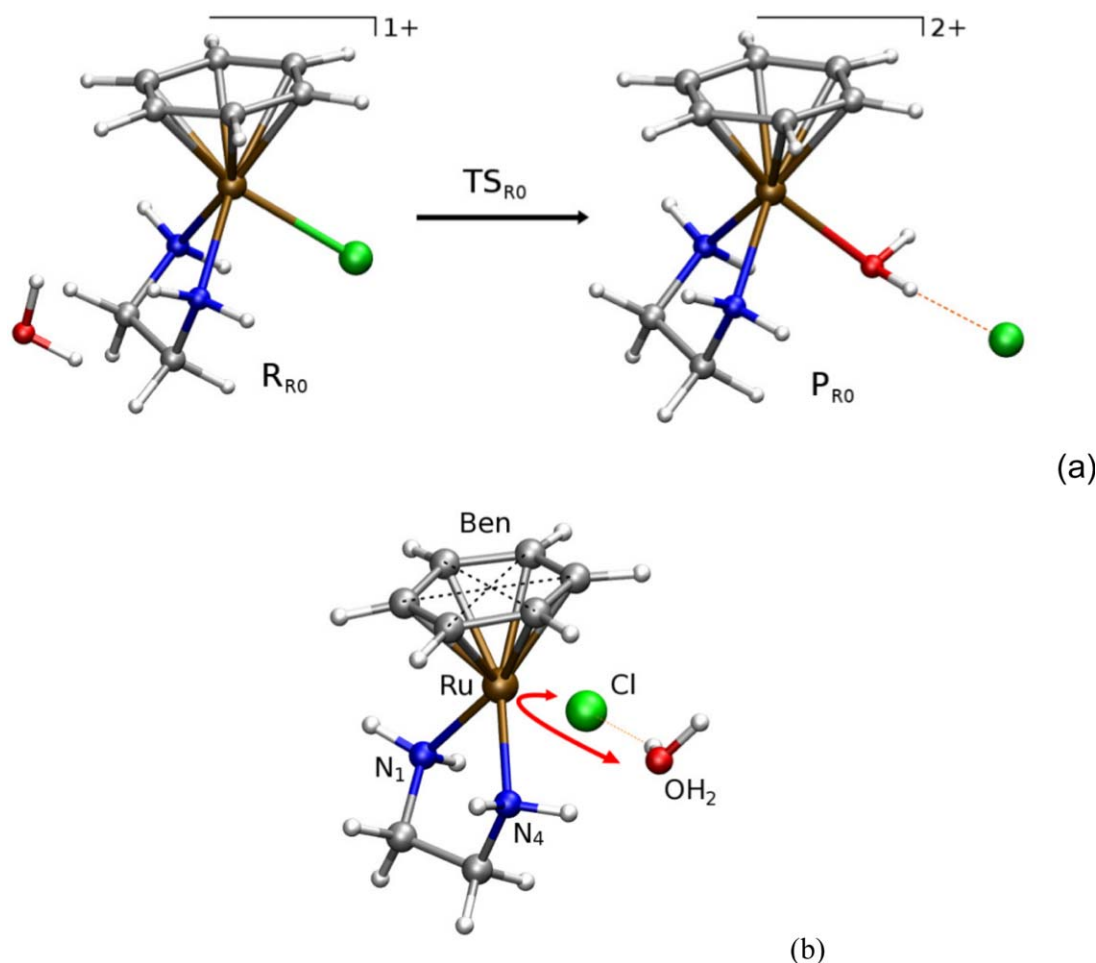


Figure 4. QM/MM optimized complexes of the hydration reaction **R0**: (a) transition from the reactant to the product, (b) transition state geometry TS_{R0} with antisymmetric stretching mode of the Cl \leftrightarrow H₂O replacement marked by red arrow.

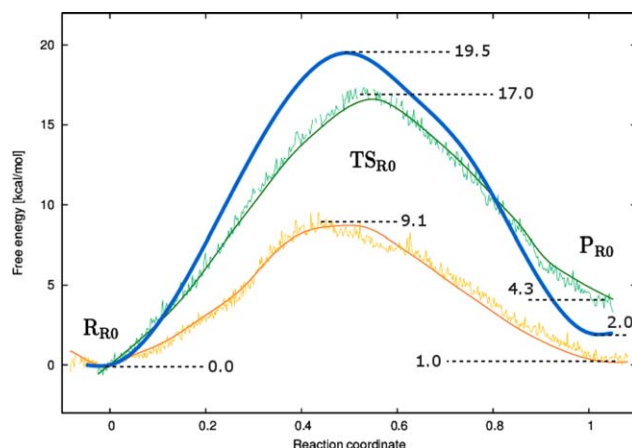


Figure 5. Free-energy profile of the hydration reaction (**R0**) computed by the umbrella sampling QM/MM MD method. The DFT(B97D)/LANL2DZ method (smooth orange curve from UI, fluctuating yellow curve from WHAM) is compared with the DFT(B3LYP)/SDD/6-31G(d) approach (smooth dark green curve from UI, fluctuating light green curve from WHAM). The latter approach is further corrected by FEP to DFT(B3LYP)/SDD/6-31++G(d,p) level (blue curve). [Color figure can be viewed in the online issue, which is available at wileyonlinelibrary.com.]

Therefore accuracy of this model is checked first on known activation and reaction energy of the hydration process. Free energy profile shown in Figure 5 was obtained by the umbrella sampling MD simulations with subsequent WHAM and UI analysis.

The B3LYP/6-31G(d) basis set with SDD pseudopotential for Ru and Cl was used for description of the QM part (green curve in Fig. 5). The free energy barrier of 17.0 and 16.6 kcal/mol were determined by WHAM and UI methods, respectively. These results are consistent with the static C-PCM model, which predicted the activation barrier of 18.1 kcal/mol.^[36] The reaction free energy is 4.3 kcal/mol (WHAM) and 4.6 kcal/mol (UI) in explicit water while the ΔG_r energy of -1.2 kcal/mol was obtained at the same level in C-PCM. This can be explained by the different nature of the computational model. In the C-PCM model, chloride anion released from $[\text{Ru}^{\text{II}}(\eta^6\text{-benzene})(\text{en})\text{Cl}]^+$ can interact only with the product complex and is stabilized by two hydrogen bonds. On the contrary, in explicit solvent, the Cl^- interacts mainly with water molecules and there is only one H-bond between Cl^- and Ru(II) complex, in average. Nevertheless, correct description of the hydration in C-PCM was also obtained using the improved quantum model, for example considering a larger basis set and more accurate computational method. In this way, $\Delta G_r = 4.4$ kcal/mol at the CCSD/6-31++G(d,p) level was acquired.^[36] Finally, the free energy profile was corrected by FEP approach to the B3LYP/SDD/6-31++G(d,p) level of the QM part with the resulting free energy barrier of 19.5 kcal/mol and the reaction energy of 2.0 kcal/mol. The barrier height is in very good agreement with the experimental value (21.1 kcal/mol), especially when we take into account the conclusions from study.^[36]

Although B3LYP functional with 6-31G(d) basis set gives satisfying results for the hydration reaction, it is not possible to use it for exploring the reaction mechanism including DNA.

The reason dwells in a lack of dispersion, which is necessary for proper description of guanine–guanine stacking interaction and partially also in the fact that this functional is computationally more demanding for the QM/MM MD simulations. Therefore, the B97D/LANL2DZ description of QM part was chosen and, for the sake of consistency, also the free energy profile for hydration reaction is constructed at this level (orange curve in Fig. 5). As it can be seen, the LANL2DZ basis set leads to substantial underestimation of both activation barrier $\Delta G_a = 9.1$ kcal/mol and reaction energy $\Delta G_r = 1.0$ kcal/mol. Small discrepancy between WHAM and UI in transition state area is caused by shape of histograms that slightly differs from Gaussian distribution in this case.

Binding to DNA

The aqua complex of $[\text{Ru}^{\text{II}}(\eta^6\text{-benzene})(\text{en})\text{H}_2\text{O}]^{2+}$, that is the product of hydration reaction, is more reactive than the original form of $[\text{Ru}^{\text{II}}(\eta^6\text{-benzene})(\text{en})\text{Cl}]^+$ complex and therefore it interacts more readily with nucleophilic active sites in biomolecules. As it is explained in introduction, binding to DNA, preferably to N7 guanine position, is important for the cytostatic activity of this complex. Such a process can occur by two reaction pathways, shown in Figure 6. One possibility is direct binding mechanism with single transition state $\text{TS}_{\text{R1}}^{\text{D}}$. In this way, also cisplatin binds to the N7 site of guanine. Alternative pathway goes through intermediate state I_{R1} , where the Ru(II) complex interacts first with guanine oxygen O6. Final stable product is the Ru-N7(G) structure.^[37,38]

We calculated all the free energy characteristics of the **R1** reaction, that is activation barriers ΔG_a and reaction energies ΔG_r , and obtained values are summarized in Table 1. In QM/MM model with explicit water box and periodic boundary conditions, the umbrella sampling method was applied to construct the free energy profile of the reactions. The QM part was treated at the lowered computational level (B97D/LANL2DZ) to keep reasonable speed of QM/MM MD simulations. The whole reaction coordinate was divided into 11 windows and within each window approximately 2.5-ps MD trajectory was evaluated. Resulting biased distributions were transformed to unbiased free energy profiles by WHAM and UI methods and these are shown for **R1** in Figure 8. Since the ΔG_a and ΔG_r energies calculated at this level of theory differ significantly from more accurate description, as we discussed above, FEP corrections to B3LYP/6-31++G(d,p) level were applied. Final reaction and activation energies are collected in the last part of Table 1, labeled as QM/MM_{corr}.

As it was already suggested by the ONIOM calculation in Ref. [38], height of the activation barrier for direct binding is almost the same as the activation barrier for the first part of two-step mechanism. In all models, the same product state **P_{R1}** is the most stable structure, uniquely preferred over **I_{R1}**. If the system gets into the **I_{R1}** state, the probability of the backward reaction to **R_{R1}** is substantially lower than for the forward transition to **P_{R1}** (barriers differ by 3 kcal/mol in QM/MM model). Thus, it can be concluded that both direct path and two-step mechanism through O6 to final N7 binding site are

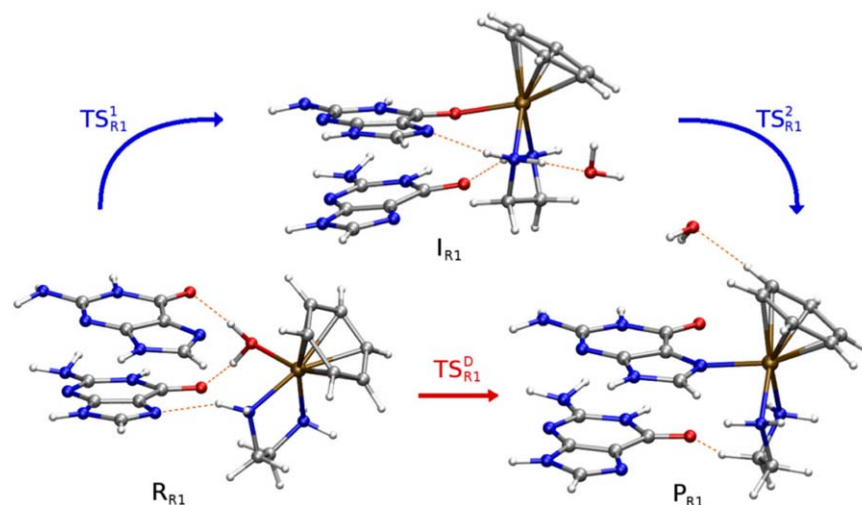


Figure 6. QM/MM optimized complexes of the Ru(II)-DNA binding process **R1**. [Color figure can be viewed in the online issue, which is available at wileyonlinelibrary.com.]

kinetically feasible and the whole process is thermodynamically spontaneous reaction.

Pronounced stability of Ru coordination to the N7 site in the **P_{R1}** structure rather than to the O6 site in the **I_{R1}** intermediate geometry corresponds to stronger nitrogen dative ability to Ru than that of oxygen. As a result, the coordination bond length between the Ru cation and the guanine binding site is shorter in **P_{R1}** and the binding interaction of the complex to the guanine pair is by about 9 kcal/mol stronger in this structure than in **I_{R1}** (see Supporting Information, Table S4–S6 for details). Transition state structures and the antisymmetric stretching vibrational modes found in **TS_{R1}^D** and **TS_{R1}¹** (see Fig. 7) indicate that the binding of Ru complex to DNA proceeds via associative mechanism as the hydration reaction discussed above. This was also confirmed by QTAIM analysis where both bond critical points (BCP) of Ru–O(Aq) and Ru–O6/Ru–N7 were located in **TS_{R1}¹**/**TS_{R1}^D** transition states (Supporting Information, Table S7). In contrast to the cross-linking studied in next sec-

tion, the benzene ligand η^6 -coordination to Ru is practically unaffected in **R1** reaction despite that different number of BCPs – 3, 4, and 5, were found in **R_{R1}**, **I_{R1}**, and **P_{R1}** structures, respectively.

Cross-link structures

The suggested reaction mechanism for the Ru(II) cross-link formation is depicted in Figure 9 where the Ru(II)-N7 monoaduct **P_{R1}**, that is product of **R1** reaction, is now initial structure. In order to keep coordination number of the Ru(II) cation equal to six, the benzene ligand has to be at least partially released when the ruthenium bridge between both N7 nitrogen is to be created. Within the reaction path, a water molecule can saturate untied valence(s). This leads to three possible cross-linked structures: (i) η^6 -coordination of the benzene ligand is transformed to η^2 -coordination and besides N7 coordination also O6 oxygen binds to Ru(II) (this structure is

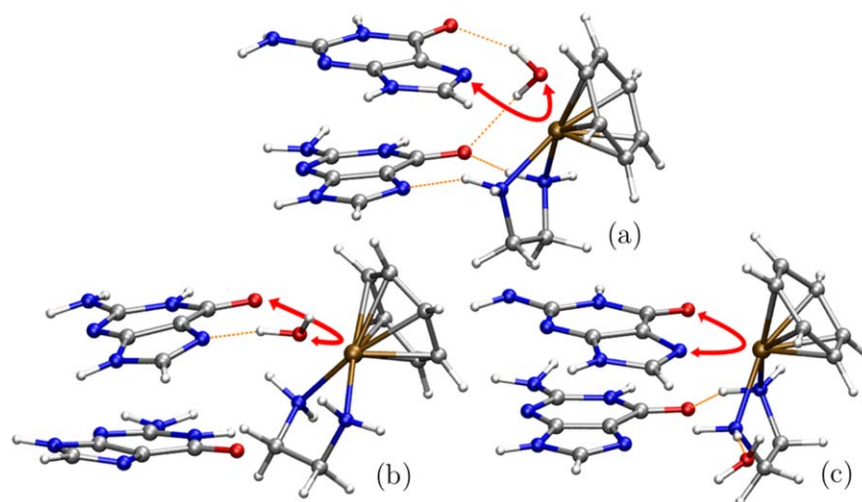


Figure 7. Transition states of the **R1** reaction mechanism: (a) **TS_{R1}²**, (b) **TS_{R1}¹**, and (c) **TS_{R1}^D**. Red arrows indicate antisymmetric stretching modes corresponding with imaginary frequency in each structure. [Color figure can be viewed in the online issue, which is available at wileyonlinelibrary.com.]

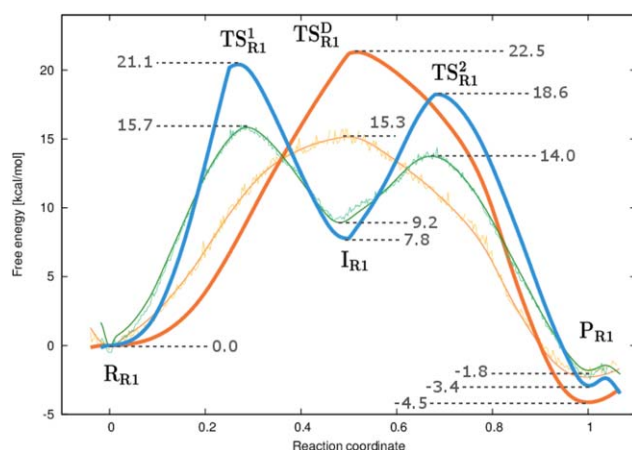


Figure 8. Free-energy profile of Ru(II) binding to DNA (**R1**) computed by the umbrella sampling QM/MM MD method. Direct binding to N7 guanine (smooth orange curve from UI, fluctuating yellow curve from WHAM, FEP corrected red curve) as well as two-step mechanism passing through O6 position (smooth dark green curve from UI, fluctuating light green curve from WHAM, FEP corrected blue curve) is shown. [Color figure can be viewed in the online issue, which is available at wileyonlinelibrary.com.]

marked as I_{R2}^2); (ii) the water molecule is coordinated to Ru(II) instead of O6 oxygen (I_{R2}^1), and (iii) the benzene ligand is fully released and both water molecule and O6 oxygen are coordinated to Ru(II) (P_{R2}). The last structure, P_{R2} , was found to be the most stable complex in this reaction mechanism.

Reaction mechanism **R2** has two possible pathways leading to final P_{R2} structure. Each of these pathways can be divided into two consequent reactions with activation barrier ΔG_a . Heights of the free energy barriers and the reaction energies ΔG_r are displayed in Table 2. Similarly to the previous reactions, the QM/MM MD umbrella sampling technique was used with the B97D/LANL2DZ description of the QM part. The resulting free energy profile is constructed by WHAM and UI methods as in the previous case and is shown in Figure 11. To get a more accurate description of the QM part, the FEP corrections using B3LYP/6-31++G(d,p) were applied on the MD samples and the final barriers and reaction energies are collected in the last column of Table 2.

From the energy profile in Figure 11, it is obvious that creation of the I_{R2}^1 cross-link with η^2 -coordinated benzene ligand and coordinated water molecule is kinetically inhibited by high-energy barrier. The barrier corresponds to rather complicated geometry of the relevant transition state TS_{R2}^{11} (Fig. 10), which indicates that the cross-link formation is quite complex process where significant structural changes occur. Interestingly, transformation of η^6 benzene coordination to η^2 occurs before TS_{R2}^{11} is reached. BE of the arene ligand is reduced from -68 to -13 kcal/mol during this process (Supporting Information, Table S9). On the contrary, the water molecule and the second guanine start to coordinate to Ru(II) at the TS_{R2}^{11} point. Also the steric repulsion of ligands in I_{R2}^1 is significant,

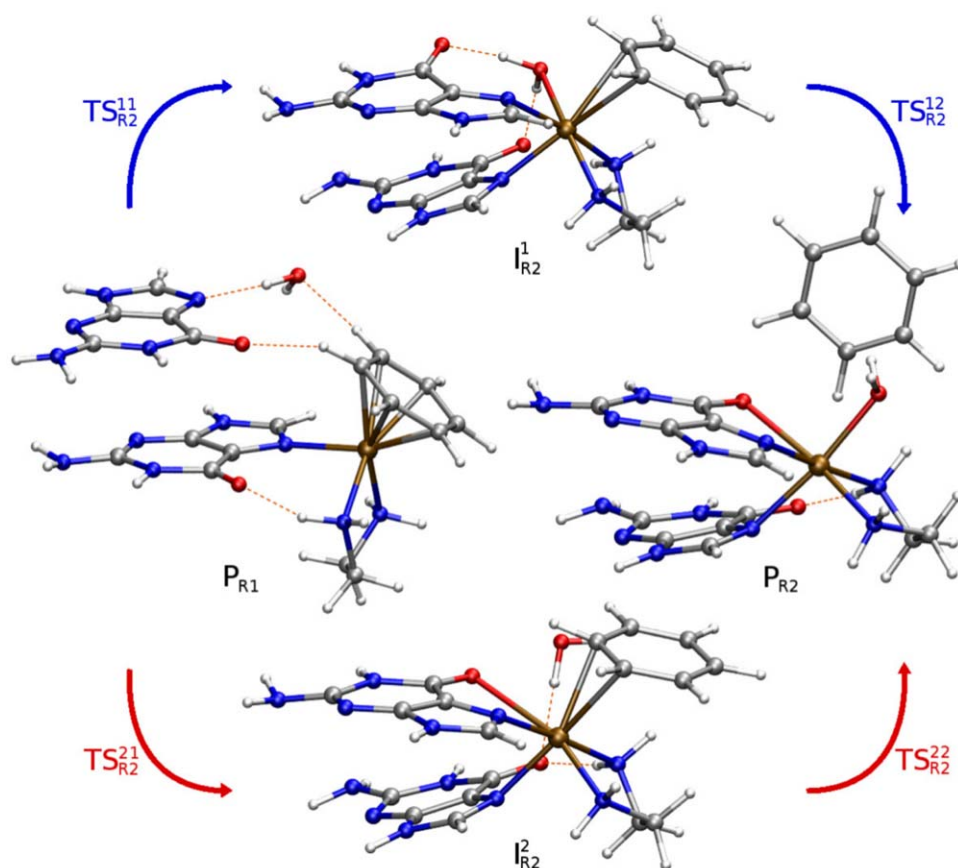


Figure 9. QM/MM optimized complexes of the cross-link formation process **R2**. [Color figure can be viewed in the online issue, which is available at wileyonlinelibrary.com.]

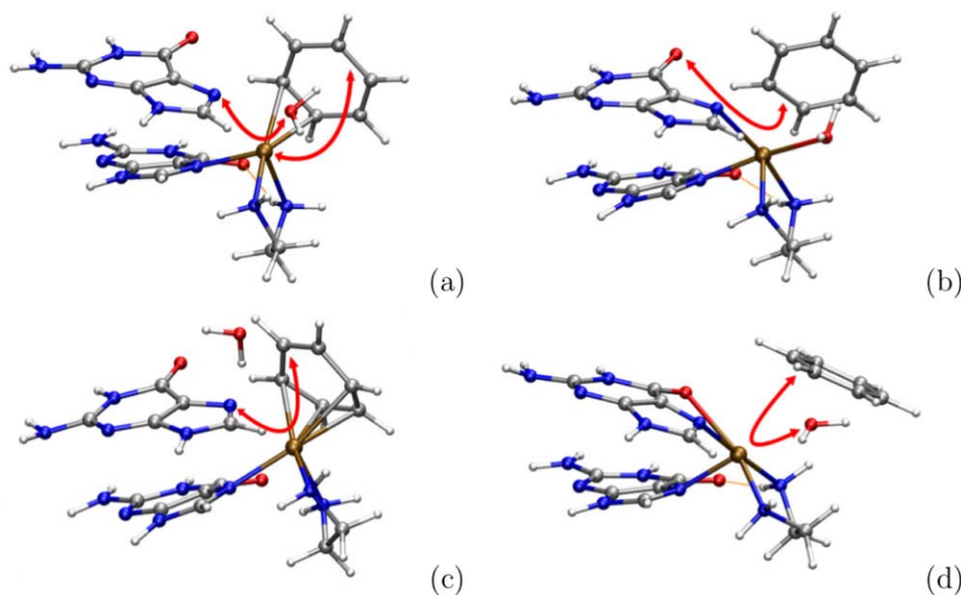


Figure 10. Transition states of the **R2** reaction mechanism: (a) TS_{R2}^{11} , (b) TS_{R2}^{12} , (c) TS_{R2}^{21} , and (d) TS_{R2}^{22} . Red arrows indicate antisymmetric stretching movements corresponding with imaginary frequency in each structure. [Color figure can be viewed in the online issue, which is available at wileyonlinelibrary.com.]

resulting in lower stability of this structure. Subsequent releasing of the benzene ligand is connected with very low barrier across the transition state TS_{R2}^{12} by antisymmetric stretching movement. This is apparent from Figure 11 where the barrier between I_{R2}^1 and P_{R2} is only 1 kcal/mol (3.2 kcal/mol with FEP corrections).

In the second reaction pathway, the I_{R2}^2 cross-linked structure is formed with partially η^2 -coordinated benzene like in I_{R2}^1 . Nevertheless, instead of water, the G2 guanine is more firmly attached to Ru(II) center partially forming the N7,O6 chelate structure. These bonding differences can be clearly detected in QTAIM analysis of the I_{R2}^2 complex (Supporting Information, Table S11). Ru-benzene BCPs in I_{R2}^2 have higher values of electron density than in I_{R2}^1 , which correlates with the weaker binding interaction of benzene in the I_{R2}^2 cross-linked structure due to the higher sterical repulsion caused by additional aqua ligand present in the coordination sphere. Formation of I_{R2}^2 structure has significantly lower transition barrier, the energy of TS_{R2}^{21} is reduced more than twice in comparison with activation barrier passing through TS_{R2}^{11} . Therefore, it can be concluded that the second reaction pathway is kinetically preferred while the first one is practically forbidden. Height of the TS_{R2}^{21} barrier is 16.9 kcal/mol in the FEP corrected QM/MM

model, which corresponds, according to Eyring TST, to the rate constant of $2.5 \text{ s}^{-1} \text{ M}^{-1}$. Therefore, the hypothetical cross-link formation should be faster process than Ru(II) binding to DNA, which can be considered as the rate controlling process.

Conclusions

Reaction mechanism of the Ru(II) piano-stool complexes was studied by the hybrid QM/MM computational technique. We chose the $[Ru^{II}(\eta^6\text{-benzene})(\text{en})\text{Cl}]^+$ complex as a representative of this group of compounds and its interactions with water and ds-DNA oligomeric model were investigated. The whole mechanism was divided into three phases: **R0**—the hydration reaction of the $[Ru^{II}(\eta^6\text{-benzene})(\text{en})\text{Cl}]^+$ complex, **R1**—binding of the resulting aqua Ru(II) complex to DNA and **R2**—subsequent formation of the intrastrand cross-linked structure between two adjacent guanines. Free energy profiles of these reactions were constructed from the umbrella sampling QM/MM MD simulations.

Hydration reaction of the Ru(II)-Cl complex, for which experimentally measured value of rate constant is available, was used for accuracy check of the B3LYP/6-31++G(d,p) description with SDD pseudopotentials. This level of theory was

Table 2. Heights of the activation barriers and the reaction energies [kcal/mol] in the cross-link formation process.

Reaction/Methods	QM(C-PCM)		ONIOM		QM/MM _{MD}		QM/MM _{corr}	
	ΔG_a	ΔG_r	ΔG_a	ΔG_r	ΔG_a	ΔG_r	ΔG_a	ΔG_r
$P_{R1} \rightarrow I_{R2}^1$	57.9	2.4	30.1	−12.8	23.8	1.1	37.0	15.3
$P_{R1} \rightarrow I_{R2}^2$	38.2	13.2	23.7	−9.7	10.1	−9.8	16.9	1.5
$I_{R2}^1 \rightarrow P_{R2}$	20.7	4.2	10.4	−8.6	1.2	−15.4	3.2	−28.8
$I_{R2}^2 \rightarrow P_{R2}$	15.2	−6.5	2.3	−11.7	8.3	−6.8	9.3	−11.2

QM/MM_{MD} stands for the umbrella sampling result at the DFT(B97D)/LANL2DZ level and QM/MM_{corr} are values corrected to DFT(B3LYP)/6-31++G(d,p) by FEP. For a comparison, ONIOM values from Ref. [38] are shown.

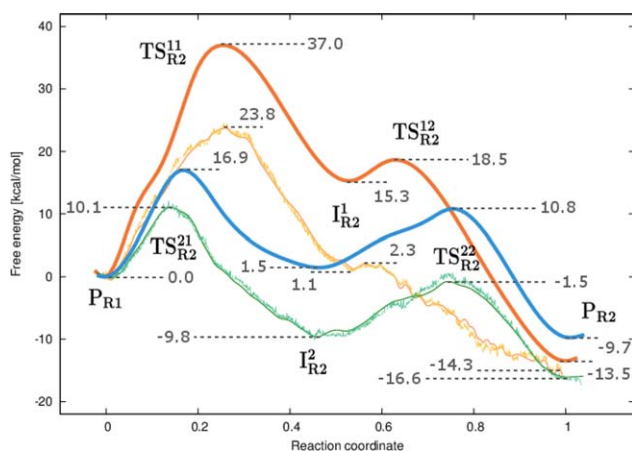


Figure 11. Free energy profile of the Ru(II) cross-link formation (R_2) computed by the umbrella sampling QM/MM MD method. Two reaction pathways going through $I_{R_2}^1$ (smooth orange curve from UI, fluctuating yellow curve from WHAM, FEP corrected red curve) or $I_{R_2}^2$ (smooth dark green curve from UI, fluctuating light green curve from WHAM, FEP corrected blue curve) to final P_{R_2} are shown. [Color figure can be viewed in the online issue, which is available at wileyonlinelibrary.com.]

chosen since additional comparison with our previous QM calculations is available. The QM/MM model with explicit water molecules provides height of the free energy barrier of 19.5 kcal/mol, which is about 0.6 kcal/mol below the experimental value.

Interaction of Ru(II) with DNA was studied in extended computational model that included 10-bp oligomer of *ds*-DNA, the Ru(II) complex, Na^+ counterions, and explicit water molecules. The QM/MM MD simulations were performed using B97D/LANL2DZ description of the QM part with FEP correction performed at the B3LYP/SDD/6-31++G(d,p) level of calculation. First, the Ru(II) coordination to the N7 atom nitrogen of guanine was explored, since N7 atom is known to be the most preferred binding site. Two possible reaction pathways were taken into account: direct substitution of the aqua ligand by N7 nitrogen and the two-step mechanism passing through the Ru(II)-O6(G) intermediate state. While the entire binding process to N7 is exergonic with the free energy change -4.5 kcal/mol, the intermediate Ru(II)-O6(G) structure is almost 8 kcal/mol above the unbound aqua complex. However, the free energy barrier for binding to O6 is by 1.4 kcal/mol lower than 22.5 kcal/mol for direct binding to the N7 position and since the transition from O6 to N7 is kinetically preferred over the backward reaction, it is apparent that both these considered pathways are feasible. The barrier heights are close to experimentally measured 20.1 kcal/mol and also prediction of the stable Ru-N7(G) structure over the Ru-O6(G) complex agrees with experimental observations.

The suggested reaction scheme for Ru(II) cross-link formation between two adjacent guanines was investigated using the same computational model. Rearrangement of the η^6 -coordinated benzene ligand to η^2 interaction followed by its full release and substitution by water molecule was assumed and the free energy changes connected with this process determined. Theoretically, the process can occur via two different


reaction pathways. However, one of them, where a sterically crowded cross-link structure coordinated simultaneously with benzene and aqua ligand, is possible neither thermodynamically nor kinetically (this process is inhibited by high free energy barrier of 37 kcal/mol). The other reaction pathway leads to the intermediate without coordinated water and is connected with relatively low free energy barrier of 17 kcal/mol. Instead of water, the remaining free valence of Ru(II) complex is saturated by O6(G2) binding. Although this structure is 1.5 kcal/mol above in free energy of the initial Ru(II)-N7(G) monoadduct, subsequent benzene replacement by water molecule (with activation barrier of 9.3 kcal/mol) is exergonic process with reaction free energy of ca 10 kcal/mol.

Acknowledgment

Access to computing and storage facilities owned by parties and projects contributing to the National Grid Infrastructure Meta-Centrum, provided under the program "Projects of Large Infrastructure for Research, Development, and Innovations" (LM2010005) is highly appreciated.

Keywords: ruthenium(II) complexes • piano-stool structure • *ds*-DNA • intrastrand cross-link • quantum mechanics—molecular mechanics • density functional theory—amber • umbrella sampling • weighted histogram analysis method • umbrella integration

How to cite this article: Z. Futera, J. V. Burda, *J. Comput. Chem.* **2014**, *35*, 1446–1456. DOI: 10.1002/jcc.23639

 Additional Supporting Information may be found in the online version of this article.

- [1] R. K. Zalups, J. Koropatnick, In *Cellular and Molecular Biology of Metals*; CRC Press; Taylor & Francis Group: New York, **2010**.
- [2] J. C. Dabrowiak, *Metals in Medicine*; Wiley, Chichester, **2009**.
- [3] M. Gielen, E. R. T. Tiekink, *Metallotherapeutic Drugs and Metal-Based Diagnostic Agents: The Use of Metals in Medicine*; Wiley: Chichester, **2005**.
- [4] P. J. Sadler, Z. Guo, *Pure Appl. Chem.* **1998**, *70*, 863.
- [5] B. Lippert, *Cisplatin: Chemistry and Biochemistry of a Leading Anti-cancer Drug*; Wiley-VCH: Weinheim, Germany, **1999**.
- [6] B. Rosenberg, L. Van Camp, T. Krigas, *Nature* **1965**, *205*, 698.
- [7] S. E. Miller, K. J. Gerard, D. A. House, *Inorg. Chim. Acta* **1991**, *190*, 135.
- [8] M. Mikola, J. Arpalahti, *Inorg. Chem.* **1994**, *33*, 4439.
- [9] K. Hindmarsch, D. A. House, M. M. Turnbull, *Inorg. Chim. Acta* **1997**, *257*, 11.
- [10] L. G. Marzilli, S. O. Ano, F. P. Intini, G. Natile, *J. Am. Chem. Soc.* **1999**, *121*, 9133.
- [11] P. N. Pavankumar, P. Seetharamulu, S. Yao, J. D. Saxe, D. G. Reddy, F. H. Hausheer, *J. Comput. Chem.* **1999**, *20*, 365.
- [12] Y. Zhang, Z. Guo, X. -Z. You, *J. Am. Chem. Soc.* **2001**, *123*, 9378.
- [13] Baik, M.-H.; R. A. Friesner, S. J. Lippard, *J. Am. Chem. Soc.* **2003**, *125*, 14082.
- [14] Z. Chval, M. Sip, *Collect. Czech. Chem. Commun.* **2003**, *68*, 1105.
- [15] J. V. Burda, M. Zeizinger, J. Leszczynski, *J. Chem. Phys.* **2004**, *120*, 1253.
- [16] J. V. Burda, M. Zeizinger, J. Leszczynski, *J. Comput. Chem.* **2005**, *26*, 907.
- [17] J. Raber, Z. Chuanbao, L. A. Eriksson, *J. Phys. Chem. B* **2005**, *109*, 11006.

- [18] H. F. Dos Santos, B. L. Marcial, C. F. De Miranda, L. A. S. Costa, W. B. De Almeida, *J. Inorg. Biochem.* **2006**, *100*, 1594.
- [19] J. K.-C. Lau, D. V. Deubel, *J. Chem. Theory Comput.* **2006**, *2*, 103.
- [20] A. Robertazzi, J. A. Platts, *Chem. Eur. J.* **2006**, *12*, 5747.
- [21] D. V. Deubel, J. Kai-Chi Lau, *Chem. Comm.* **2006**, *23*, 2451.
- [22] T. Zimmermann, J. V. Burda, *Dalton Trans.* **2010**, *39*, 1295.
- [23] M. Iwamoto, S. Mukundan, L. G. Marzilli, *J. Am. Chem. Soc.* **1994**, *116*, 6238.
- [24] P. M. Takahara, C. A. Frederick, S. J. Lippard, *J. Am. chem. Soc.* **1996**, *118*, 12309.
- [25] S. M. Cohen, Y. Mikata, Q. He, S. J. Lippard, *Biochem.* **2000**, *39*, 11771.
- [26] J. Graham, M. Mushin, P. Kirkpatrick, *Nat. Rev. Drug. Discov.* **2004**, *3*, 11.
- [27] R. Canetta, M. Rozenzweig, S. K. Carter, *Cancer Treat Rev.* **1985**, *12*, 125.
- [28] S. C. Allardyce, J. P. Dyson, *Platin Met Rev* **2001**, *45*, 62.
- [29] R. E. Morris, R. E. Aird, P. del Socorro Murdoch, H. Chen, J. Cummings, N. D. Hughes, S. Parsons, A. Parkin, G. Boyd, D. I. Jodrell, P. J. Sadler, *J. Med. Chem.* **2001**, *44*, 3616.
- [30] F. Wang, H. Chen, S. Parsons, I. D. H. Oswald, J. E. Davidson, P. J. Sadler, *Chem. Eur. J.* **2003**, *9*, 5810.
- [31] R. Fernández, M. Melchart, A. Habtemariam, S. Parsons, P. J. Sadler, *Chem. Eur. J.* **2004**, *10*, 5173.
- [32] Y. K. Yan, M. Melchart, A. Habtemariam, P. J. Sadler, *Chem. Commun.* **2005**, 4764.
- [33] A. F. A. Peacock, A. Habtemariam, R. Fernandez, V. Walland, F. P. A. Fabbiani, S. Parsons, R. E. Aird, D. I. Jodrell, P. J. Sadler, *J. Am. Chem. Soc.* **2006**, *128*, 1739.
- [34] V. Brabec, O. Novakova, *Drug. Res. Upd.* **2006**, *9*, 111.
- [35] A. M. Pizarro, P. J. Sadler, *Biochimie* **2009**, *91*, 1198.
- [36] Z. Futera, J. Klenko, J. E. Sponer, J. Sponer, J. V. Burda, *J. Comput. Chem.* **2009**, *30*, 1758.
- [37] C. Gossens, I. Tavernelli, U. Rothlisberger, *J. Phys. Chem. A* **2009**, *113*, 11888.
- [38] Z. Futera, J. A. Platts, J. V. Burda, *J. Comput. Chem.* **2012**, *33*, 2092.
- [39] Gaussian 09, M. J. Frisch, G. W. Trucks, H. B. Schlegel, G. E. Scuseria, M. A. Robb, J. R. Cheeseman, G. Scalmani, V. Barone, B. Mennucci, G. A. Petersson, H. Nakatsuji, M. Caricato, X. Li, H. P. Hratchian, A. F. Izmaylov, J. Bloino, G. Zheng, J. L. Sonnenberg, M. Hada, M. Ehara, K. Toyota, R. Fukuda, J. Hasegawa, M. Ishida, T. Nakajima, Y. Honda, O. Kitao, H. Nakai, T. Vreven, J. A. Montgomery, Jr., J. E. Peralta, F. Ogliaro, M. Bearpark, J. J. Heyd, E. Brothers, K. N. Kudin, V. N. Staroverov, R. Kobayashi, J. Normand, K. Raghavachari, A. Rendell, J. C. Burant, S. S. Iyengar, J. Tomasi, M. Cossi, N. Rega, N. J. Millam, K. Klene, J. E. Knox, J. B. Cross, V. Bakken, C. Adamo, J. Jaramillo, R. Gomperts, R. E. Stratmann, O. Yazyev, A. J. Austin, R. Cammi, C. Pomelli, J. W. Ochterski, R. L. Martin, K. Morokuma, V. G. Zakrzewski, G. A. Voth, P. Salvador, J. J. Dannenberg, S. Dapprich, A. D. Daniels, O. Farkas, J. B. Foresman, J. V. Ortiz, J. Cioslowski, Fox, Gaussian, Inc., Wallingford CT, D. J. **2009**.
- [40] D. A. Case, T. A. Darden, T. E. Cheatham, C. L. Simmerling, J. Wang, E. D. R.; R. Luo, K. M. Merz, B. Wang, D. A. Pearlman, M. Crowley, S. Brozell, V. Tsui, H. Gohlke, J. Mongan, V. Hornak, G. Cui, P. Beroza, C. Schafmeister, J. W. Caldwell, W. S. Ross, P. A. Kollman, Amber 8, University of California, San Francisco, **2004**.
- [41] M. W. Schmidt, K. K. Baldrige, J. A. Boatz, S. T. Elbert, M. S. Gordon, J. H. Jensen, S. Koseki, N. Matsunaga, K. A. Nguyen, S. Su, T. L. Windus, M. Dupuis, J. A. Montgomery, Jr. *J. Comput. Chem.* **1993**, *14*, 1347.
- [42] R. Ahlrichs, M. Bär, M. Häser, H. Horn, C. Kölmel, *Chem. Phys. Lett.*, **1989**, *162*, 165.
- [43] H. J. Werner, P. J. Knowles, R. Lindh, F. R. Manby, M. Schutz, P. Celani, T. Korona, A. Mitrushenkov, G. Rauhut, T. B. Adler, R. D. Amos, A. Bernhardsson, A. Berning, D. L. Cooper, M. J. O. Deegan, A. J. Dobbyn, F. Eckert, E. Goll, C. Hampel, G. Hetzer, T. Hrenar, G. Knizia, C. Köppl, Y. Liu, A. W. Lloyd, R. A. Mata, A. J. May, S. J. McNicholas, W. Meyer, M. E. Mura, A. Nicklass, P. Palmieri, K. Pflüger, R. Pitzer, M. Reiher, U. Schumann, H. Stoll, A. J. Stone, R. Tarroni, T. Thorsteinsson, M. Wang, A. Wolf, MolPro, version 2006.1, a package of ab initio programs, 2008.
- [44] S. Dapprich, I. Komaromi, K. S. Byun, K. Morokuma, M. Frish, J. J. *Mol. Struct. (Theochem)* **1999**, *462*, 1.
- [45] D. C. Liu, J. Nocedal, *Math Program* **1989**, *45*, 503.
- [46] L. Verlet, *Phys. Rev.* **1967**, *159*, 98.
- [47] W. C. Swope, H. C. Andersen, *J. Chem. Phys.* **1982**, *76*, 637.
- [48] H. C. Andersen, *J. Chem. Phys.* **1980**, *72*, 2384.
- [49] H. J. C. Berendsen, J. P. M. Postma, W. F. van Gunsteren, A. DiNola, J. R. Haak, *J. Chem. Phys.* **1984**, *81*, 3684.
- [50] D. Frenkel, B. Smit, Understanding Molecular Simulation: From Algorithms to Applications; Elsevier, London, **1996**.
- [51] G. M. Torrie, J. P. Valleau, *Chem. Phys. Lett.* **1974**, *28*, 578.
- [52] G. M. Torrie, J. P. Valleau, *J. Comput. Chem.* **1977**, *23*, 187.
- [53] J. Kaestner, *Comput. Mol. Sci.* **2011**, *1*, 932.
- [54] S. Kumar, J. M. Rosenberg, D. Bouzida, R. H. Swendsen, P. A. Kollman, *J. Comput. Chem.* **1992**, *13*, 1011.
- [55] M. Souaille, B. Roux, *Comput. Phys. Commun.* **2001**, *135*, 40.
- [56] J. Kaestner, W. Thiel, *J. Chem. Phys.* **2005**, *123*, 144101.
- [57] J. Kaestner, W. Thiel, *J. Chem. Phys.* **2006**, *124*, 234106.
- [58] W. Zhang, T. Hou, C. Schafmeister, W. S. Ross, D. A. Case, AmberTools version 1.4, **2010**.
- [59] J. Wang, R. M. J. W. Wolf, P. A. Caldwell, Kollman, D. A. Case, *J. Comput. Chem.* **2004**, *25*, 1157.
- [60] C. I. Bayly, P. Cieplak, W. Cornell, P. A. Kollman, *J. Phys. Chem.* **1993**, *97*, 10269.
- [61] W. D. Cornell, P. Cieplak, C. I. Bayly, P. A. Kollman, *J. Am. Chem. Soc.* **1993**, *115*, 9620.
- [62] P. Cieplak, W. D. Cornell, C. Bayly, P. A. Kollman, *J. Comput. Chem.* **1995**, *16*, 1357.
- [63] T. Fox, P. A. Kollman, *J. Phys. Chem. B* **1998**, *102*, 8070.
- [64] W. L. Jorgensen, J. Chandrasekhar, J. D. R. W. Madura, Impey, M. L. Klein, *J. Chem. Phys.* **1983**, *79*, 926.
- [65] D. Andrae, U. Haussermann, M. Dolg, H. Stoll, H. Preuss, *Theor. Chim. Acta* **1990**, *77*, 123.
- [66] D. Andrae, U. Haussermann, M. Dolg, H. Stoll, H. Preuss, *Theor. Chim. Acta* **1991**, *78*, 247.
- [67] A. Bergner, M. Dolg, W. Kuchle, H. Stoll, H. Preuss, *Mol. Phys.* **1993**, *80*, 1431.
- [68] Y. Duan, C. Wu, S. Chowdhury, M. C. Lee, G. Xiong, W. Zhang, R. Yang, P. Cieplak, R. Luo, L. Taisung, J. Cladwell, J. Wang, P. Kollman, *J. Comput. Chem.* **2003**, *24*, 1999.
- [69] D. A. Case, T. A. Darden, T. E. Cheatham, C. L. Simmerling, J. Wang, R. E. Duke, R. Luo, R. C. Walker, W. Zhang, K. M. Merz, B. Roberts, B. Wang, S. Hayik, A. Roitberg, G. Seabra, I. Kolossvary, K. F. Wong, F. Paesani, J. Vanicek, J. Liu, X. Wu, S. Brozell, T. Steinbrecher, H. Gohlke, Q. Cai, X. Ye, J. Wang, M. J. Hsieh, G. Cui, D. R. Roe, D. H. Mathews, M. G. Seetin, C. Sagui, V. Babin, T. Luchko, S. Gusarov, A. Kovalenko, P. A. Kollman, Amber 11, University of California, San Francisco, **2010**.
- [70] P. J. Hay, W. R. Wadt, *J. Chem. Phys.* **1985**, *82*, 270.
- [71] W. R. Wadt, P. J. Hay, *J. Chem. Phys.* **1985**, *82*, 284.
- [72] P. J. Hay, W. R. Wadt, *J. Chem. Phys.* **1985**, *82*, 299.
- [73] T. H. Dunning, Jr., P. J. Hay, *Mod. Theor. Chem.* **1976**, *3*, 1.
- [74] R. F. W. Bader, *Pure Appl. Chem.* **1988**, *60*, 145.
- [75] R. F. W. Bader, H. Essen, *J. Chem. Phys.* **1984**, *80*, 1943.
- [76] R. F. W. Bader, Atoms in Molecules: A Quantum Theory; Clarendon Press: Oxford, UK, **1990**.
- [77] F. Y. Wang, A. Habtemariam, van der E. P. L. Geer, R. Fernandez, M. Melchart, R. J. Deeth, R. Aird, S. Guichard, F. P. A. Fabbiani, P. Lozano-Casal, I. D. H. D. I. Oswald, Jodrell, S. Parsons, P. J. Sadler, *Proc Natl Acad Sci USA* **2005**, *102*, 18269.

Received: 6 February 2014
Revised: 23 April 2014
Accepted: 2 May 2014
Published online on 28 May 2014